EXPLORING TRANSIENT PH, OXYGEN, AND DOPAMINE NEUROTRANSMISSION *IN VIVO* WITH FAST-SCAN CYCLIC VOLTAMMETRY

Jennifer Lee Ariansen

A thesis submitted to the faculty of the University of North Carolina at Chapel Hill in partial fulfillment of the requirements for the degree of Masters Degree in the Curriculum in Neurobiology

Chapel Hill
2011

Approved by:

Dr. R. Mark Wightman, Ph.D

Dr. Regina M. Carelli, Ph.D

Dr. A. Leslie Morrow, Ph.D

ABSTRACT

JENNIFER LEE ARIANSEN: Exploring Transient pH, Oxygen, and Dopamine Neurotransmission *In Vivo* with Fast-Scan Cyclic Voltammetry
(Under the direction of R. Mark Wightman)

Dopamine projections that extend from the ventral tegmental area to the striatum have been implicated in the biological basis for behaviors associated with reward, addiction, and neurodegenerative disorders, such as Parkinson's disease. Many techniques have been employed to monitor these neurochemical and neurophysiological changes. In this study we utilized fast-scan cyclic voltammetry to monitor transient pH and oxygen changes in the striatum of primates. Dopamine release was observed in a small number of locations, but this signal was masked by the overarching pH changes. Oxygen and pH are coupled in the brain through a complex system of blood flow and metabolism as a result of transient neural activity. Indeed, this balance is at the heart of imaging studies such as functional magnetic resonance imaging (fMRI). We observed increases in pH to the cue onset and increases in oxygen to predicted reward delivery, respectively. Additionally, acidic pH changes were observed following probability predicted reward delivery and to the cue onset in a small percentage of cases. These findings show that pH, oxygen, and dopamine can be measured in primate striatum and have implications linking blood flow and metabolism to neural activity.

ACKNOWLEDGEMENTS

I would like to first thank my mentor, Dr. R. Mark Wightman. Thank you for your guidance through the years and the ways that you have facilitated my fascination with science. Thank you also for the PBRs.

I have worked with many colleagues throughout my years in the Wightman Lab. I would like to start by thanking Dr. Gina Carelli, who first took me on as a work study student in 2003 and has provided endless support since then. I would also like to thank numerous members of both the Wightman and Carelli labs who contributed to this work: Dr. Paul Phillips, Dr. Michael Heien, Dr. Andre Hermans, Dr. Richard Keithley, and Dr. Pasha Takmakov. I thank our collaborators at Cambridge University, Dr. Wolfram Schultz, Dr. Istvan Hernandi, and Dr. Maria Bermudez. I would also like to thank Elyse Dankoski, Dr. Nina Owesson-White, Dr. Zoe McElligott, and Dr. Parastoo Hashemi for their continued support, scientific and otherwise, throughout the writing process. Thank you to the numerous faculty that have participated in my development as a scientist on and off the bench.

I would also like to thank my chosen family whose support is immeasurable in a world full of measurements. Thank you for offering a treasured balance to this work.

I also want to recognize the animals that were used in this study as models for human biology that also taught me about the human condition.

Thank you to the space between.

TABLE OF CONTENTS

LIST OF FIGURES

LIST OF ABBREVIATIONS

BOLD	Blood oxygen level dependent
CF	Center fixation spot
cm	Centimeter
CS	Conditioned stimulus
DA	Dopamine
fMRI	Functional magnetic resonance imaging
FSCV	Fast scan cyclic voltammetry
µm	Micrometer
µM	Micromolar
mL	Milliliter
ms	Millisecond
nA	Nanoamperes
NAc	Nucleus accumbens
nM	Nanomolar
PBS	Phosphate buffered saline
PET	Positron emission tomography
s	Second
SEM	Scanning electron microscopy
t	Time
TTL	Transistor transistor logic
US	Unconditioned stimulus
V_{max}	Maximal rate of uptake

V	Volts
VTA	Ventral tegmental area

CHAPTER 1

THE NEUROBIOLOGY OF THE MESOLIMBIC DOPAMINE SYSTEM

Introduction

The human brain has approximately 100 billion neurons that form close to 1000 trillion synapses (Herculano-Houzel, 2009). Despite the overwhelming complexity of the brain, it's connections and synapses, the scope of reward-related brain processes has narrowed to the study of the mesolimbic dopamine pathway (Wise, 2004). Indeed, a strong body of research exists linking dopamine neuronal firing and subsequent dopamine release to cues and rewards associated with those cues (Di Chiara and Imperato, 1988; Schultz et al., 1997; Hyland et al., 2002; Phillips et al., 2003; Roitman et al., 2004; Wise, 2004; Stuber et al., 2005; Ikemoto, 2007; Owesson-White et al., 2008). Neural activity and dopamine release do not exist in a vacuum or a beaker, though. In the brain, transient neural activity causes a cascade of local changes to maintain homeostasis, and pH changes are an important marker of neuronal activity and subsequent metabolic processes that underlie the originations of behavior (Chesler, 2003; Takmakov et al., 2010). Indeed, understanding the complex organization of brain metabolism, oxygen delivery and subsequent pH changes in concert with dopamine release is the key to relating brain mechanics to behavior. The primary focus of this thesis is to elucidate further the neural mechanisms at work during reward related behaviors in the mesolimbic dopamine system in behaving primates. This chapter will review general mesolimbic system anatomy and neurochemistry as well as the techniques used to collect the data presented in Chapter Two.

Anatomy of the mesolimbic dopamine system

The mesolimbic dopamine system originates in the ventral tegmental area (VTA) of the midbrain and extends to areas of the forebrain including the nucleus accumbens (NAc), caudate/putamen, and prefrontal cortex (Haber and Fudge, 1997; Fields et al., 2007; Ikemoto, 2007). Of particular importance are the projections that extend from the VTA to the dorsal and ventral striatum, two anatomically semi-distinct subunits of the striatum (Figure 1.1). Dopaminergic cell bodies in the VTA are thought to comprise up to 55 % of the neuronal population (Margolis et al., 2006). Dopamine neurons can be characterized by their thin, unmylineated processes that exhibit high thresholds of activation, their relatively long action potentials, and clear after hyperpolarizations (Grace and Onn, 1989; Nowak and Bullier, 1998; Onn et al., 2000). Dopamine neurons display two firing modes: tonic and phasic. The tonic firing is pacemaker-like and in the range of 2-11 Hz. The phasic activations are ≥ 20 Hz, and burst fire in response to salient stimuli (Overton and Clark, 1997; Schultz et al., 1997). In fact, upon repeated pairings of salient stimuli and rewards, these neurons burst fire to both the cue and the reward (Schultz et al., 1997; Hyland et al., 2002; Owesson-White et al., 2009). Even more interesting is the fact that the phasic activity of these neurons is not observed in tissue slice experiments, suggesting an intrinsic role for the VTA in burst firing (Shepard and Bunney, 1988; Sombers et al., 2009).

Having a link between dopamine cell body firing in the VTA and subsequent terminal release, the origins (or terminations of, depending on your perspective) of dopamine release in striatum can be considered. The tonic firing pattern of dopamine neurons is thought to underlie the basal concentrations of dopamine, which is estimated to be ~5-20 nM (Parsons and Justice, 1992). The burst firing activity can lead to transient concentration increases of up to 1 µM (Garris et al., 1997; Robinson et al., 2001; Venton et al., 2003b).

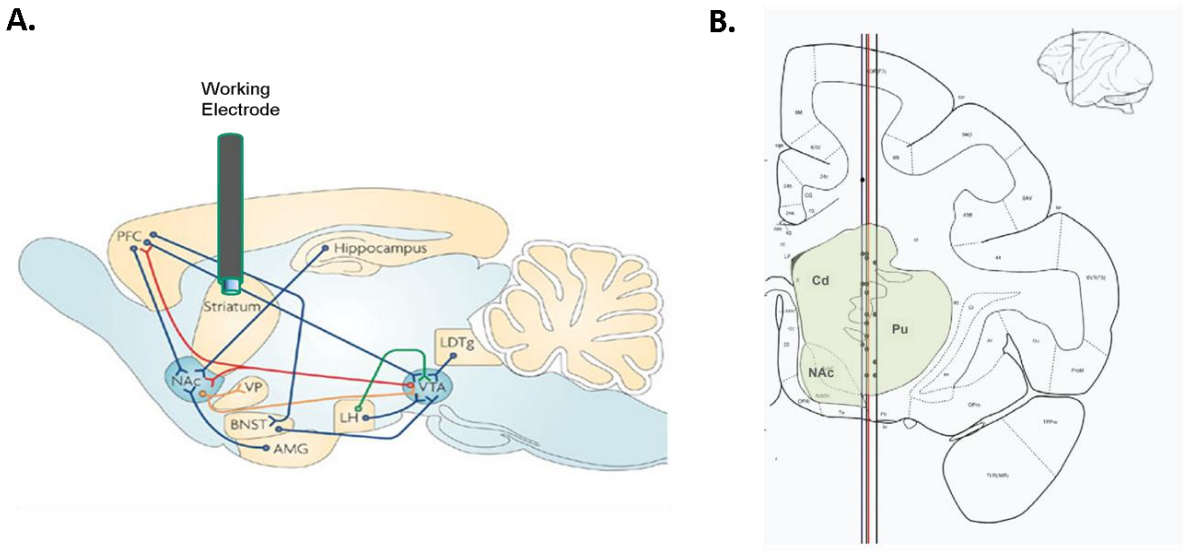

Figure 1.1. Mesolimbic dopamine anatomy. A. Sagittal view of the rodent mesolimbic dopamine system (red). The working electrode is lowered into the striatum or nucleus accumbens on the day of the experiment. Modified figure from (Kauer and Malenka, 2007). B. Coronal view of primate caudate, putamen, and nucleus accumbens with electrode placements along dorsal/ventral track. Modified figure from (Paxinos, 2000).

Upon release dopamine acts a volume transmitter as it diffuses out of the synaptic cleft into the extracellular space to act on presynaptic and postsynaptic targets. The dopamine transporter lies on the membrane of the presynaptic neuron and is responsible for transporting extracellular dopamine back into the presynaptic terminals (Wightman et al., 1988; Cragg and Rice, 2004). Inhibiting these transporters causes elevated levels of dopamine in the synapse and is responsible for the euphoric and addictive effects of drugs of abuse like cocaine and amphetamine (Di Chiara and Imperato, 1988; Jones et al., 1999). Dopamine that is not taken up by the transporter interacts with presynaptic autoreceptors or postsynaptically on GABAergic receptors (Garris et al., 2003).

Dopamine receptors are G-protein coupled receptors that are divided into two categories based on their excitatory or inhibitory intracellular cascades (Kebabian and Calne, 1979) . Upon activation of the D1-like receptors, the D1 and D5 subclasses, which are coupled to G_s G-proteins, adenylate cyclase levels are increased which in turn increases the second messenger, cyclic adenosine monophosphate (cAMP) (Brown and Makman, 1972). In contrast, D2-like receptors, D2, the D3, and D4 subclasses, are $G_{i/o}$ coupled and decrease cAMP production because their inhibitory effects on adenyl cylcase (De Camilli et al., 1979). Both D1-like and D2-like receptors are expressed postsynaptically, but have different affinities for dopamine. The D1-like receptors exhibit a low-affinity for dopamine, and so, require relatively high concentrations to become activated. The D2-like receptors exhibit a high affinity for dopamine and can be activated by low concentrations of dopamine (Richfield et al., 1989). Also, the D2-like receptors are present presynaptically, acting as autoreceptors to inhibit neurotransmitter synthesis and release (Schmitz et al., 2001; Wu et al., 2002). Both receptor subtypes are present in the striatum and most likely play a role in reinforcing behaviors, though

research has not led to a consensus on the exact role for either subtype (Ikemoto et al., 1997).

Techniques for measuring pH, dopamine and oxygen

Measuring pH, neurotransmitter concentration, and oxygen changes in the brain during behavior require techniques to measure local, transient concentration changes in the extracellular space. It has been postulated that neural activity causes changes in brain pH through the complex balance of metabolism and blood flow (Chesler, 2003). Indeed, alkaline shifts have been measured in the rat cortex following stimulation as a result of CO_2 removal because of increased blow flow (Urbanics et al., 1978). *In vitro* slice experiments in the rat hippocampus reveal alkaline pH shifts post-stimulation as well (Chen and Chesler, 1992b, a). Traditional *in vivo* approaches to measuring oxygen in the extracellular space have utilized the Clark style electrode which reduces oxygen at a platinum surface (Clark et al., 1953) and have been made in the cerebellum during local field potential stimulations (Caesar et al., 2008). *In vivo* experiments measuring oxygen have led to many of the theories behind imaging techniques such as positron emission tomography (PET), which measures blood flow, and blood oxygen level dependent functional magnetic resonance imagining (BOLD fMRI), which measures blood oxygenation (Fox et al., 1986; Raichle, 1998; Ances, 2004). Both techniques are non-invasive and can be used on humans, but lack the spatial and temporal resolution of electrochemical techniques.

The most common method of measuring dopamine *in vivo* is microdialysis (Westerink, 1995). Microdialysis is a diffusion-based sampling method that provides excellent neurotransmitter selectivity *in vivo*, but offers concentration information in the extracellular space on the order of minutes to hours. So, microdialysis is regularly used to measure tonic neurotransmitter concentration over a long period of time and is not

suited well for measuring transient changes, and causes significant tissue damage in the brain over time (Lu et al., 1998; Jaquins-Gerstl and Michael, 2009).

Fast scan cyclic voltammetry has been employed to measure all three species *in vivo* (Stamford et al., 1984; Runnels et al., 1999; Venton et al., 2003b; Roitman et al., 2004; Takmakov et al., 2010), but has only been performed in primate brain slices to date (Cragg et al., 2000). The technique works by measuring current changes at the carbon-fiber microelectrode of analytes as they are oxidized and reduced after voltage application. The current changes can be converted to concentrations when compared to known concentrations *in vitro*. Of the electrochemical techniques used for *in vivo* behavior experiments, fast-scan cyclic voltammeter (FSCV) provides the best chemical and time scale resolution for measuring transient changes in the brain (Robinson et al., 2003). In primate recordings, FSCV was used in conjunction with a modified carbon-fiber microelectrode that measured more than 12 cm in length, was well insulated over 85% of this length with glass with a diameter of less than 175 µm, and were sufficiently rugged to penetrate the dura mater and scar tissue associated with repeated measurements (Heien, 2005)(see Electrode Methods Chapter 2). An SEM image of these is shown in Figure 1.2 (Hermans, 2007).

To measure transient fluctuation in analyte concentrations *in vivo*, the carbon fiber is inserted into the brain region of interest, in this case the dorsal striatum, and a triangular potential is applied to the electrode usually every 100 ms in a triangular fashion at a high scan rate (400 V/s). The limits of the positive and negative excursions are chosen to oxidize and reduce the analyte of interest within the potential window. The fast scan rate causes a large background current attributable to the charging of the double-layer capacitance of the electrode, but because it is fairly stable, it can be digitally subtracted from the analyte signal. The resulting faradaic current can then be plotted against the applied waveform potential to produce a background-subtracted

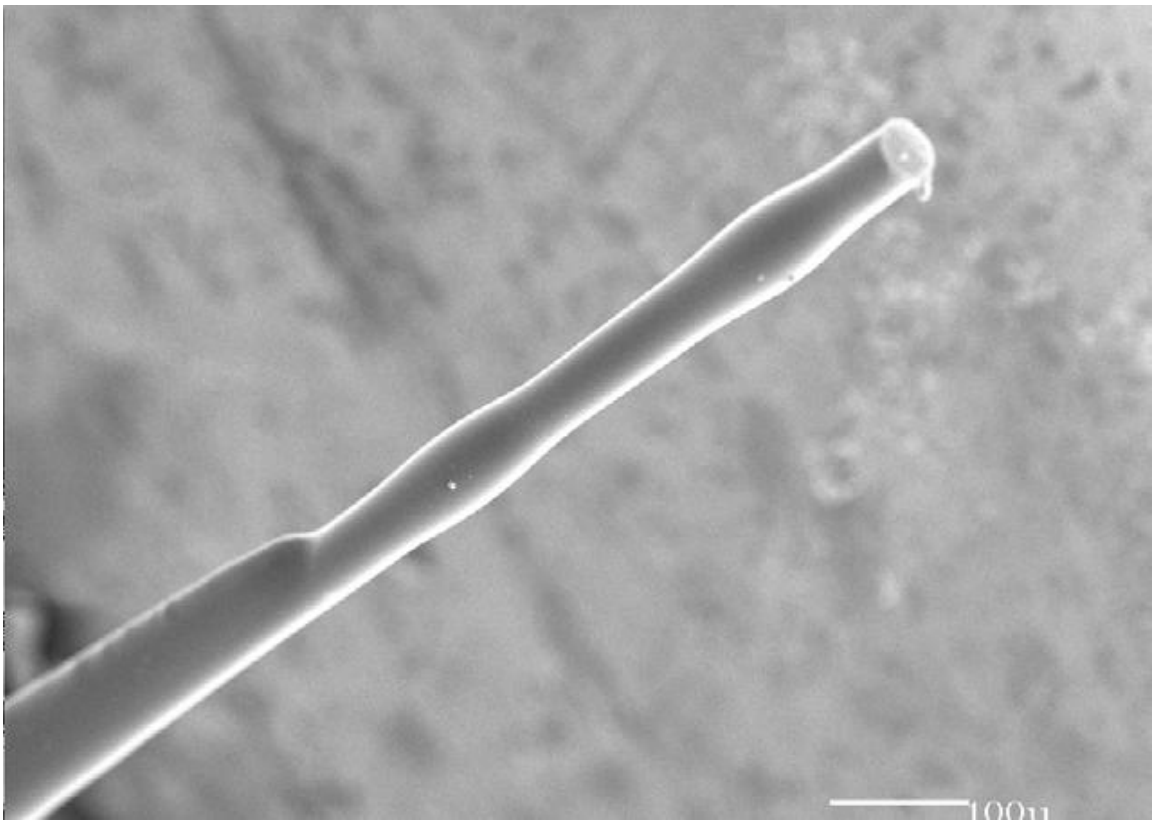

Figure 1.2. SEM image of electrodes for primate recordings. SEM image of a 33 µm carbon fiber attached to an etched tungsten wire encased in a glass capillary.
*courtesy of Andre Hermans

cyclic voltammogram. This voltammogram, with peaks marking the oxidation and reduction of the species of interest, serves as a signature for the qualitative identification of electroactive compounds (Kawagoe et al., 1993; Cahill et al., 1996; Keithley et al., 2011). FSCV is a differential technique that cannot be used to measure absolute values, but instead, measures changes in currents that can be converted into a concentration using an *in vitro* calibration factor (Robinson et al., 2003; Heien, 2005). To date, FSCV is the only technique that can provide *in vivo* information in the extracellular space with sufficient temporal, spatial, and chemical resolution (Figure 1.3).

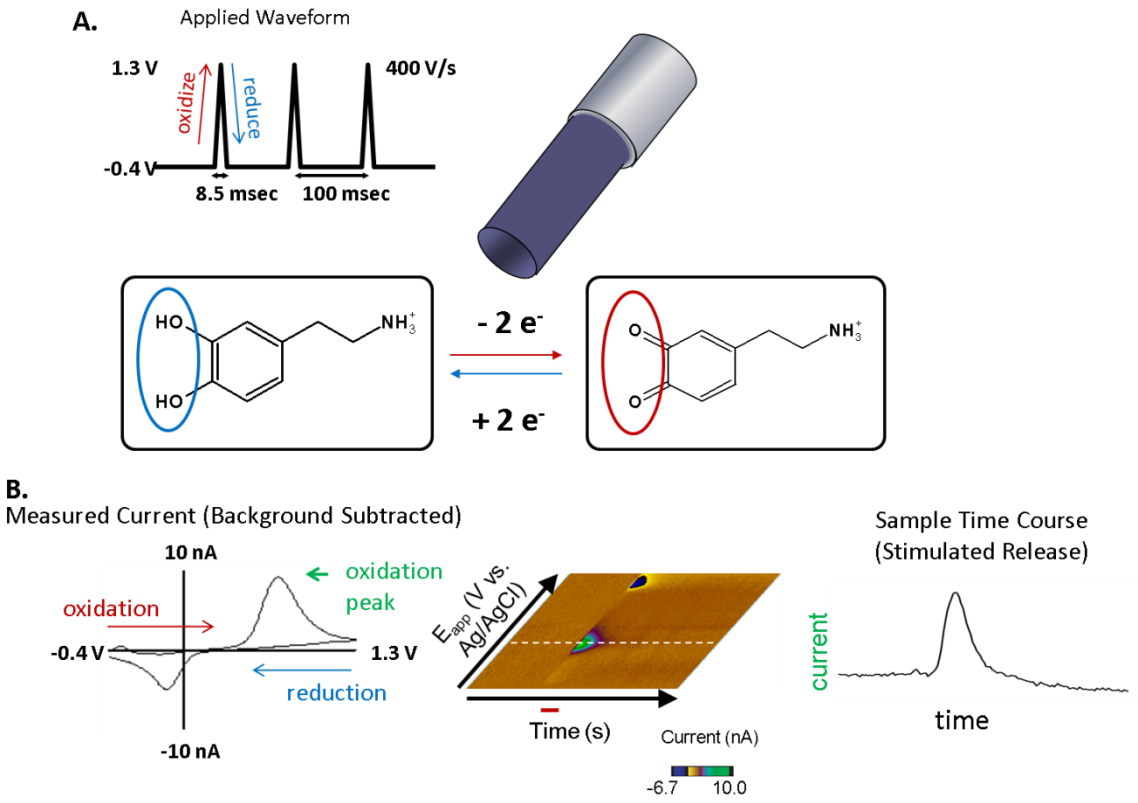

Figure 1.3. **Fast-scan cyclic voltammetry.** A. The triangular waveform is applied to the electrode with excursions of -0.4V to 1.3V sufficient enough to oxidize (red) dopamine at ~0.6V (red) to dopamine ortho-quinone and reduce dopamine ortho-qunione back to dopamine at -0.2V (blue). The waveform is applied at 400V/s every 100 msec lasting for 8.5 msec. B. The resulting faradic current (in nA) applied against the waveform application (in V) to generate a cyclic voltammogram. The voltammograms can be plotted in false color plotted against time and applied potential to produce a color plot. A subsequent current vs time trace taken from horizontal dotted white line shows the current increase from the oxidation peak (green). The peak current can later be converted to a concentration using an *in vitro* factor for the electrode.

CHAPTER 2

EXPLORING TRANSIENT PH, OXYGEN, AND OPAMINE NEUROTRANSMISSION *IN VIVO* WITH FAST-SCAN CYCLIC VOLTAMMETRY

Introduction

The events in the brain that occur following the presentation of a reward or a cue that predicts a reward have been studied at length in recent years. The focus of much of the research has been on the mesolimbic dopamine system (Di Chiara and Imperato, 1988; Schultz et al., 1997; Hyland et al., 2002; Roitman et al., 2004; Wise, 2004; Stuber et al., 2005; Ikemoto, 2007; Owesson-White et al., 2009). Common methods for measuring neural activity during reward are electrophysiology, electrochemistry, and functional magnetic resonance imaging (fMRI). Each technique provides insight into different components of neural activity associated with reward and reinforcing behaviors. Indeed, electrophysiological data has shown that dopamine neurons originating in the ventral tegmental area are immediately activated by unexpected rewards and cues that predict rewards (Fiorillo et al., 2003; Tobler et al., 2005). Blood oxygen level dependent (BOLD) fMRI measures the level of blood oxygenation that is governed by neural activity and blood flow in the brain. The response time of this technique is slower, on the order of seconds, because the 'hemodynamic filter' of this physiological response delays the signal (Ogawa et al., 1990; Bandettini et al., 1993; Aguirre et al., 1998). Despite the sluggish timescale resolution of BOLD fMRI, it has shown activation in the human dorsal and ventral striatum and the prefrontal cortex, further implicating these brain regions in reward and utility theory (O'Doherty, 2004; Tobler et al., 2007; Tobler et al., 2009). Electrochemical recordings offer insight into neurotransmitter and oxygen concentrations as well as pH in the extracellular space with subsecond temporal resolution (Cahill et al.,

1996; Runnels et al., 1999; Venton et al., 2003a; Hashemi et al., 2009; Park et al., 2009), but are invasive techniques not utilized in humans.

Until recently, it has been difficult to reconcile these three techniques and the information they give us about the complex balance of energy utilization and neural activity and the subsequent physiological responses such as blood flow and oxygen consumption which cause local, transient pH changes in the brain in response to cues and rewards. In short, neural activity in response to rewards or reward-predicting cues is thought to increase blood flow that causes increases in oxygen levels and clearance of CO_2. Removal of CO_2 causes alkaline pH shifts. In balance with this mechanism, increases in metabolism cause increases in CO_2 and lactic acid production causing an acidic pH shift (Kaila, 1998; Chesler, 2003; Venton et al., 2003a; Takmakov et al., 2010). Voltammetric recordings in primate brain slices have only recently been reported (Cragg et al., 2000, 2002). Catecholamine release has been shown in the caudate of primates during Pavolvian reward conditioning, but was collected using amperometry and as such, chemical validation that the signal is dopaminergic is inconclusive (Yoshimi et al., 2011). In the current study, we peer into this research area where electrophysiology, BOLD fMRI, and electrochemistry meet and begin to draw conclusions about the role of pH at the subsecond, synaptic level during reward based activities in the primate striatum.

EXPERIMENTAL SECTION

Chemicals

All chemicals were purchased from Sigma-Aldrich (St. Louis, MO) and used as received. Solutions were prepared using doubly distilled water (Megapure system, Corning, New York). For flow injection experiments phosphate buffered saline (150 nM

NaCl, 10 mM Na_2HPO_4,1.2 mM $CaCl_2$) was used. Stock solutions of dopamine were prepared in 0.1 M HCl, and were diluted to the desired concentration with phosphate-buffered saline buffer on the day of use. Tungsten etching was performed in 1.0 N NaOH solution, saturated with $NaNO_2$. The diazonium salt, 4-sulfobenzenediazonuim tetrafluoroborate, was synthesized as previously described (Hermans et al., 2006).

Electrodes

The carbon-fiber microelectrodes were fabricated from two different types of carbon fibers: 12 µm diameter carbon fibers (Thornel P55, Amoco, Greenville, SC) and 33 µm diameter carbon fibers (Textron Systems Division, Wilmington, MA). These electrodes differed from those traditionally used in rats in that they had a tungsten wire (125 µm diameter, 15 cm length, Advent research Materials, Oxford, England) as a support. The tips of tungsten wires were etched to a tip in etching solution and were cleaned by applying 4.0 V in electrocleaning solution (Grobet USA, Carlstadt, NJ)(Hermans and Wightman, 2006). Carbon-fibers were attached along the whole length of the tungsten wire with conductive silver epoxy (Epo-tek, Billerica, MA) extending from the tip of the tungsten wire approximately 2 cm. After the epoxy cured, the tungsten wire and carbon fiber were inserted into a glass capillary and pulled in a horizontal electrode puller (Narishige, East Meadow, NY). The end of the capillary which held the etched portion of the tungsten wire and carbon fiber with 2 cm excess was mounted into the stationary end of the puller. After the heating element reached a temperature sufficient to soften the glass, the movable capillary holder, which held the non-etched end of the tungsten wire, was slowly pulled resulting in a very thin (~5µm) glass-insulating layer over the whole length of the tungsten wire with attached carbon fiber. The diameter of the electrode assembly, tungsten wire support rod, carbon fiber, and glass-insulating layer, was approximately 150 µm.

The assembly was inspected under a microscope to ensure a smooth transition of the glass over the tip of the tungsten wire and the carbon fiber and that the glass-insulating layer was consistently smooth throughout the length of the electrode. Additionally, the carbon fiber and the glass were cut with a scalpel blade approximately 250 µm from the end of the tungsten tip. Another insulating layer was applied to the electrode tips with Epoxylite insulation (The Epoxylite Corporation, St. Louis) at 40°C for 1 minute (Verhagen et al., 2003) and then slowly withdrawn (1 mm/10 s). The electrodes were cured for 8 hours at 80°C.

Post-curing, the electrodes were polished at a 25° angle on a micropipette beveler (Sutter instrument, Novato, CA). The electrodes were then cycled in PBS buffer from -0.4V to 1.3 V vs. Ag/AgCl and the background current was examined to ensure that the electrodes were well insulated. In addition, this pretreatment activates the electrode (Heien et al., 2003a)

Following the electrochemical pretreatment P-55 microelectrodes were coated with 4-sulfobenzene by applying a potential of -1V Vs Ag/AgCl to the electrode for 5 minutes in a 3 mM solution of 4-sulfobenzenediazonium tetrafluoroborate dissolved in 0.1M HCl (Hermans et al., 2006). Electrodes manufactured from 33µm diameter fiber did not undergo this treatment. Lastly, both types of electrodes were dip-coated with Nafion as described previously (Kawagoe et al., 1993) and the response to acidic and basic pH shifts and known dopamine concentrations was assessed with a flow-injection apparatus.

Flow-injection apparatus

Prior to *in vivo* experimentation, each electrode was tested in known concentrations of dopamine and acidic and basic pH shifts via a flow-injection apparatus. The electrode was positioned at the outlet of a 6-port rotary valve (Rheodyne model

5041 valve). The analyte was loaded into an injection loop and delivered to the surface of the electrode following manual switching of the 6-pot valve. The solution flow rate was approximately 2 ml/s and was driven by syringe pump or gravity.

In vivo recordings

In vivo experiments were performed in collaboration with Wolfram Schultz and coworkers in Cambridge, England. The experimental design is similar to experiments reported previously (Tobler et al., 2003; Tobler et al., 2005; Bermudez and Schultz, 2010). Recordings were made in 3 Macaca mulatta monkeys that were mildly fluid deprived (~200 mL liquid/ day). All procedures were performed in Cambridge, complied with the Animal Protection Law, and were supervised by the Veterinary Office.

Voltammetric recordings were made in the caudate, putamen, and cortex. The reward was a sweetened liquid delivered by a computer-controlled solenoid valve from a spout at the animal's mouth in fixed quantities of around 0.2 ml. Licking behavior was monitored with an infrared detector.

Experimental Design

Presentation of predictable reward

Animals were trained in a Pavlovian task in which different visual stimuli coded the probability (p=0.05, 0.50, or 0.90) of subsequent reward delivery. Three different visual cues were presented in a unique place on the computer screen and were easily discriminated, although they were similar in physical salience. Each trial was initiated by a center fixation spot (CF) shown on a computer screen approximately 20 inches from the animal's face. The eye movement to this spot was monitored by a separate camera. Following the appearance of the CF, the monkey was required to perform a keytouch within 500 ms. One of the three cues indicating the probably of the reward appeared between 1.5 and 2 sec after the keytouch. Another 1.5 seconds later the color of the CF

changed from red to green, prompting the monkey to release the keytouch. The reward was delivered to the animal's mouth one second after the key was released. The computer screen went blank 500 ms after the reward was delivered and the next trial was initiated 3.5 ± 0.5 seconds later. This procedure was continued for 90 trials. A timing diagram for this behavioral task can be seen in Figure 1.

Presentation of free reward

Unpredicted reward was delivered in a separate block of trials that consisted of 15 consecutive trials. The time between each reward delivery was 4 seconds plus an exponentially distributed interval with a mean of 5 seconds. Thus, inter-trial intervals ranged from 5 to 13 seconds and averaged 9 seconds. The time between each block of trials was at least 30 minutes. The free reward trial was performed for every of the 51 recording locations after successful completion of the 90 predicted reward trials. During data analysis, the 15 responses at each location were averaged around the time of reward delivery.

Recordings were conducted in 27 striatal regions in Animal 1 and in 23 striatal and 3 cortical locations in Animal 2, and 3 striatal locations in Animal 3. The recording locations were confirmed by histological examination of stereotaxically oriented coronal brain sections. In each location approximately 90 single trials were performed, resulting in around 30 trials for each given probability (p=0.05, p=0.50, and p=0.95, respectively). Given this number for each location only 1 or 2 rewarded 5% trials and 1 or 2 non-rewarded 95% trials were recorded.

Data acquisition and analysis

Fast-scan cyclic voltammograms were acquired and analyzed using locally constructed hardware and software written in LabVIEW (National Instruments, Austin, TX) that has been described previously (Michael et al., 1999; Heien et al., 2003b). The

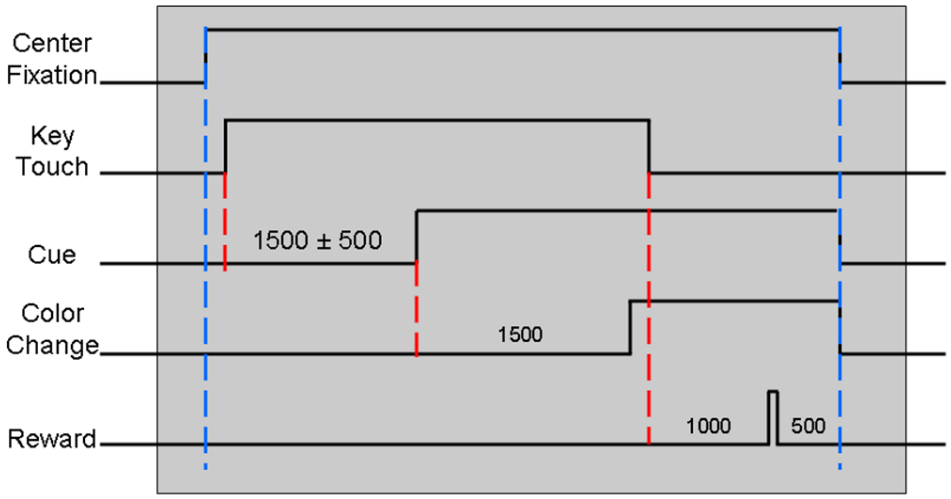

Figure 2.1. Behavioral task performed by monkeys for a predicted reward. Each trial begins with the center fixation and cues the monkey to touch a key touch within the next 500m s. If the key touch is not performed, then the trial is aborted. After an interval of 1.5 s ± 0.5 s a cue is presented that codes for either p=0.05, p=0.50, or p=0.95 of reward. 1.5 seconds after the cue is presented the center fixation light changes cueing the animal to release the key touch. For rewarded trials, the juice reward was presented 1.0 second later. The next trial is initiated 3.5 ± 0.5 s after a completed trial.

*figure courtesy of Andre Hermans

system was modified to run on a laptop computer for portability (Forry et al., 2004). Triangular excursions were normally from -0.6V or -0.4 V vs. Ag/AgCl to 1.0 V and 1.4V at a scan rate of 400 V/s. For experiments in which oxygen was measured the waveform began with a scan from 0V to +.8V, a reversal to -1.4V, and the returned to 0.0 V. The waveforms were repeated at a frequency of 10 Hz. The recorded signal was filtered at 10 kHz before being digitized. The behavior was synchronized to the voltammetric recordings by measuring TTL pulses at the onset of each event in the behavioral sequence.

Color representations were used to visualize the data (Michael et al., 1998) with the applied potential as ordinate and time as abscissa. The current is represented on a non-linear color scale to visualize the changes in current. Cyclic voltammograms were sorted according to specific recording locations and the experimental paradigm, and then background subtraction and signal averaging was performed.

RESULTS

Responses to pH changes and dopamine at carbon fiber microelectrodes

Changes in pH and dopamine can be measured by carbon fiber microelectrodes with background subtracted cyclic voltammetry (Runnels et al., 1999; Robinson et al., 2003). Representative responses are shown in Figure 2. In Figure 2A and B, the response to a bolus of 0.3 acidic pH and 0.3 basic pH relative to absolute 7.4 pH is shown. In response to this solution, the current changed at several potentials as seen in the color plot and cyclic voltammogram. The color plot contains all of the cyclic voltammograms in the 15 s measurement interval. The response to acidic and basic solutions has been previously characterized, and it was found that the current at -0.3 V on the negative going scan is most useful for tracking pH changes (Takmakov et al., 2010). This peak is referred to as the Q peak because it resembles that for reduction of

a quinone. In Figure 2C the response to a bolus of 2 µM dopamine (Figure 2C) is shown using the -4V to 1.3V waveform. In Figure 2D the response to 2 µM dopamine and 37.5 µM oxygen is shown using a 0V to .8V to -1.4V to 0V waveform. The color plot shows the current changes of these electrodes in false color relative to the applied potential and time for each. The current at the Q-peak of the acidic and basic pH changes and at the oxidation peak for dopamine are presented in the first row of Figure 2A, B, and C (horizontal dotted line across color plot). Representative cyclic voltammograms for each condition are taken along the vertical line in the color plot. The cyclic voltammograms for acidic and basic pH changes are similar to voltammograms reported previously with the same scan parameters (Takmakov et al., 2010; Heien et al., 2003a). The background currents recorded at these electrodes ranged from 100 nA to 300 nA. On average, the sensitivity of these electrodes was 8 ± 3 nA / µM dopamine (n=8 electrodes, ± SEM) and 4.1 ± 0.12 nA / +0.3 pH and -4.6 ± 0.13 nA / -0.3 pH at the Q-peak. The detection limit of these electrodes is approximately 15 nM with noise values of approximately 0.04 nA.

The 33 µm electrodes showed similar responses to each condition. The background currents at these electrodes ranged from 500 nA to 1500 nA. The average sensitivity for these electrodes was 13 ± 4 nA/ µM dopamine (n=7 electrodes, ± SEM) and 4.35 ± .15 nA/ +.03 and -.03 pH**.** The typical noise value of these electrodes was approximately 0.1 nA yielding a detection limit of approximately 25 nM. Both types of electrodes were polished to 25º to increase surface area. The electroactive surface area of the 12 µm electrodes was approximately 0.3 x 10^{-5} cm^2 and was 2 x 10^{-5} cm^2 for the 33 µm electrodes. For each condition similar signals have been measured following: electrical stimulation of dopamine neurons *in vivo*, drug administration, or rewarding or aversive tastants (Venton et al., 2003a; Heien et al., 2005).

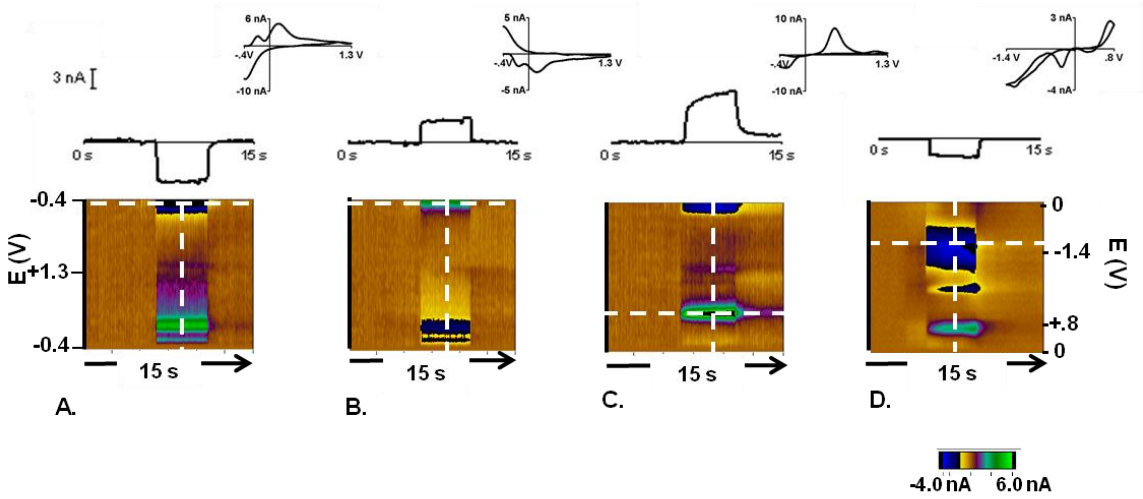

Figure 2.2. *In vitro* measurements for each species with a 12 µm carbon fiber electrode. Cyclic voltammogram (CV) (top, inset) representing the current change by applied potential during the bolus injection of the analyte.. The CV Is used to identify chemical species *in vivo. The* line graph shows the current fluctuation during the 15 s injection at the peak potential of interest.
The color plot shows all changes in current (in false color, greens are positive changes, blues are negative changes) at various applied potentials (y-axis) over time (x-axis) (Michael et al., 1998) . Current fluctuations for acidic and basic pH changes are best viewed at the Q-peak at -0.3 V on the cathodic scan of the triangular waveform -0.4V to +1.3V (A,B). DA oxidation occurs at +0.65 V on the anodic scan with the waveform -0.4V to +1.3 (C). For the potential window between -1.4V and +0.8V dopamine oxidation can be viewed at +0.65V and the oxygen reduction can be viewed at -1.2V. A. The response to a bolus of –0.3 pH units relative toan absolute of 7.4 from PBS buffer with HCL. Three peaks are generated and the horizontal line indicates the potential at which current changes were evaluated. The negative current change averaged ~4 nA/-0.3 pH unit relative to absolute 7.4 pH. B. The response to a bolus of +0.3 pH units relative to an absolute of 7.4 from PBS buffer with NaOH. As in (A), three peaks were generated and positive current changes at the -0.3 V potential (horizontal line on the color plot) indicated a basic pH change. The average response to this bolus was ~4 nA/+0.3 pH units relative to absolute 7.4 pH. C. The response to a bolus of 2 µM dopamine . The potential at which current changes occurred in response to this bolus was +0.65V (horizontal line) and these responses averaged ~ 4 nA/2 µM dopamine . D. The response of the electrode to a bolus of 2 µM dopamine and 37.5 µM O_2 performed with the waveform excursions of 0.0 V to 0.8V to -1.4V. The response to DA was ~3 nA/ 2 µM and ~ 3 nA/ 37.5 µM O_2, respectively.

Dopamine-like signal and oxygen responses

In Animal 3, a set of experiments with the experimental design as in Figure 1 were conducted, but employee the waveform that allows detection of both dopamine and oxygen signals (Figure 2D). Figure 3 shows color plots averaged to the cue and current versus time traces for the responses observed with this waveform. In this set of experiments the cue predicted a 50% probability of reward. The responses in Figure 3A were recorded during rewarded trials whereas the responses in Figure 3B were recorded in unrewarded trials. A dopamine-like signal following the reward delivery and at a slightly later time there was an oxygen increase. The dopamine-like response was not present in unrewarded trials and the oxygen increase was prolonged (Figure 3B). Following the cue there was a very small, ~0.1nA dopamine-like response, for both rewarded and unrewarded trials. These responses are the average of those obtained in the caudate during three recording days totaling 36 trials. The data is not presented in concentration because post-calibrations were not performed with these electrodes.

pH and catecholamine changes during free reward

Figure 4 shows a representative color plot and concentration trace average for 15 trials obtained during free reward in Animal 1. In this and all remaining experiments described here, the -0.4 to 1.3 waveform was used. The data was averaged to the reward presentation that occurs at the 0 s timestamp. The background was taken from averaged scans between 0.5 s to 1.5 s before the reward was delivered. Cyclic voltmm0grams for each type of response are presented in the inset of the Figure A, B, and C. There were two types of responses: a long term acidic shift lasting for approximately 5 seconds following the reward observed in ~90% of recordings (31 locations)(Figure 4B) and a no significant change in pH following free reward in ~10% of recordings (2 locations)(Figure 4A). In all free reward trials, there were always one of these two responses.

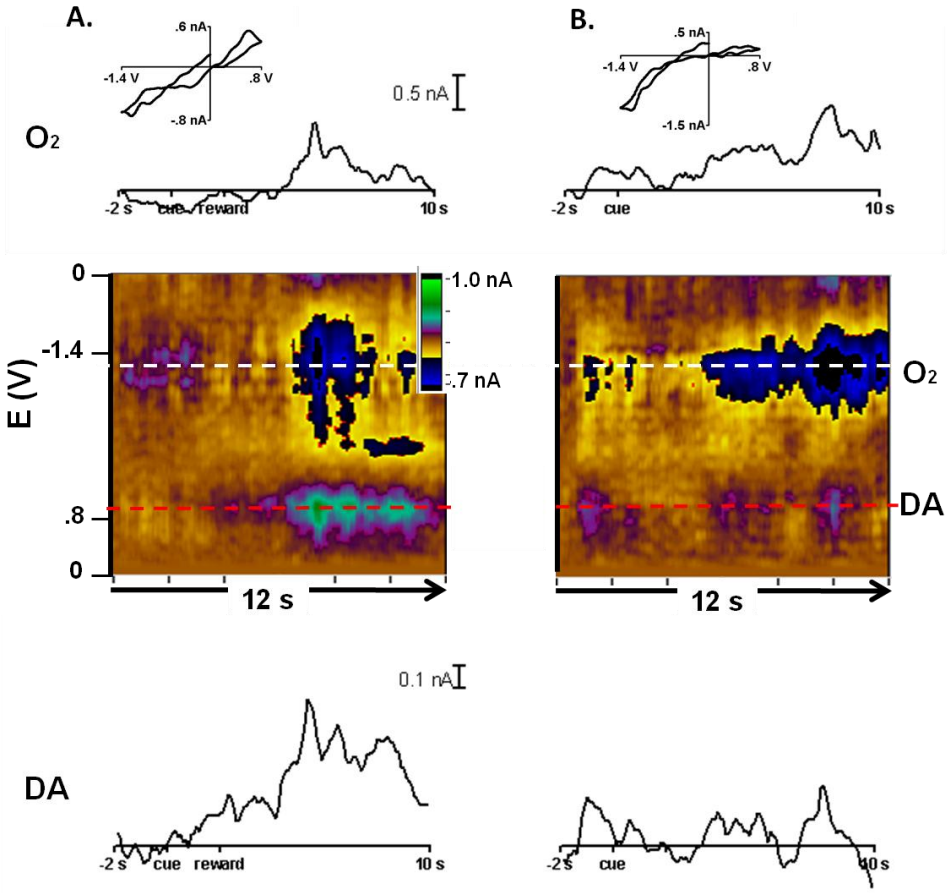

Figure 2.3. Dopamine-like signal and oxygen increases in p=0.50 trials. Current v time trace, color plot and representative cyclic voltammogram for dopamine and O_2. A. Reward trials averaged to the cue at 0 s. The current vs time trace for O_2 (horizontal white line in color plot) and dopamine (red in color plot) . Below: the average color plot of 22 rewarded trials in which the cue predicted a 50% probability of reward. The cyclic volammogram (inset) was taken at 6.5 s. B. Current vs time trace for O_2 (white) and dopamine (red) and average color plot of 14 unrewarded trials in which the cue predicted a 50% probability of reward. The cyclic voltammogram (inset) was taken at 8 s.

The large pH changes during free reward obfuscated the dopamine signal in the striatum of these primates. To resolve a dopaminergic signal from these data, principal component regression (PCR), was conducted (Heien et al., 2004; Keithley et al., 2009). The signal obtained for the pH shift was used as the first and only principal component to perform PCR. Following PCR, all non-used principal components (the residual) were used to construct a color plot. Interestingly, an oxidative current can be seen at the potential where the oxidation of dopamine is expected. It occurs immediately following the delivery of the unpredicted juice reward (Figure 4C). By plotting the current at the oxidation potential for dopamine versus time, a time course for a dopamine-like signal is obtained (Figure 4C, top panel). Evaluating the residual in this way, a dopamine-like signal could be observed in 14% of the striatal recording locations.

pH changes during the presentation of predicted rewards

To examine pH changes during the predicted-reward task (simplified Figure 5C), the voltammetric data were averaged around each of the distinct events (appearance of the color fixation spot (CF), presentation of the reward-predicting cue (CS), and the time of reward delivery (US)) at a single location. Additionally, data from each location were sorted according to the reward probability, p=0.05, p=0.50, or p=0.95 and to the occurrence (or lack) of reward delivery. The data presented are averaged to the CS and sorted by rewarded or unrewarded trials. Rewarded trials for the data where the cue predicted a 5% probability of reward have been discarded so that only unrewarded trials are presented (top panel Figure 3A). Likewise, unrewarded trails for the data where the cue predicted a 95% probability of reward have been discarded (bottom panel Figure 5A). The trials where the 50% probability of reward cue have been divided into unrewarded and rewarded categories (Figure 5A, rows 2 and 3, respectively).

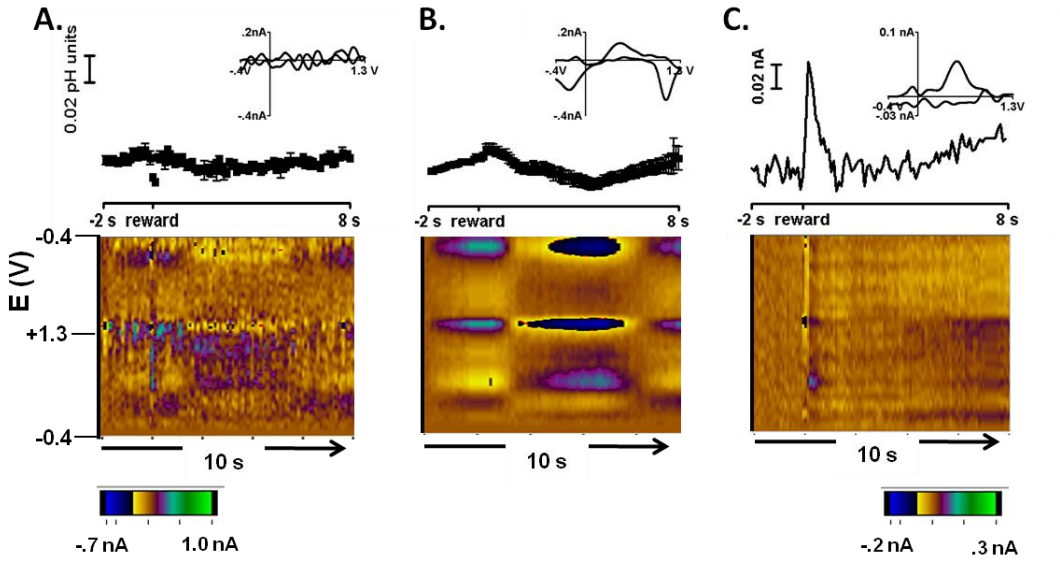

Figure 2.4. Free reward response . A. Representative cyclic voltammogram (top, inset), concentration vs time (middle), and average color plot at two locations where there was no change following the free reward.
B. Representative cyclic voltammogram (top, inset), concentration vs. time (middle), and average color plot representation of the response in about 90% of the recording locations . C. Cyclic voltammogram (top, inset), current vs time (middle), and color plot of a dopamine-like signal after the removal of pH.

Three types of responses were observed, a short term basic pH shift, a short-term basic pH shift followed by an acidic pH shift, and an acidic pH shift. All three types of responses were observed with the different reward probability types and are represented in concentration versus time traces and average color plots (Figure 5A, rows 1, 2, 3, and 4). Cyclic voltammograms for a basic pH shift and acidic pH shift are shown as insets in Figure 5. Figure 5D summarizes the percentage of occurrences by reward probability type. A short term basic shift was the most predominant signal, occurring in 75-83% of the recording locations, regardless of cue probability type or rewarded or unrewarded trials (blue section, Figure 5C). Acidic pH changes were also observed. An acidic pH change following a basic pH change was observed in every reward probability scenario, occurring 15-27% of recordings (turquoise section, Figure 5C). Acidic changes not associated with the cue presentation or a preceding basic pH shift were observed in approximately 18% of recordings overall (green section, Figure 5C). No change was observed in some cases, but no more than 8% for any given cue probability reward type (purple section, Figure 5C).

Interestingly, in recordings where a short term basic shift was observed, the peak amplitudes across probability of reward showed a general increasing trend by probability of reward, 5% probability of reward showed a 0.035 ± 0.006 (n=38 ± SEM) basic pH shift, 50% probability of reward showed a 0.038 ± 0.005 (n=57 ± SEM) basic pH shift, and 95% probability of reward showed a 0.042 ± 0.011 (n=31 ± SEM) basic pH shift, respectively (Figure 6A). These three conditions were significantly ($p=0.0197$, student's T test) greater than the basic pH shift observed in during unpredicted reward, 0.017 ± 0.005 (n=36 ± SEM), but were not significantly different from one another, suggesting a correlation of basic pH shifts in the brain to cues associated with reward. Additionally, there was no significant difference or trend in the later acidic shift following a basic shift (Figure 6B). Lastly, we compared the long term acidic shift amplitude by relative

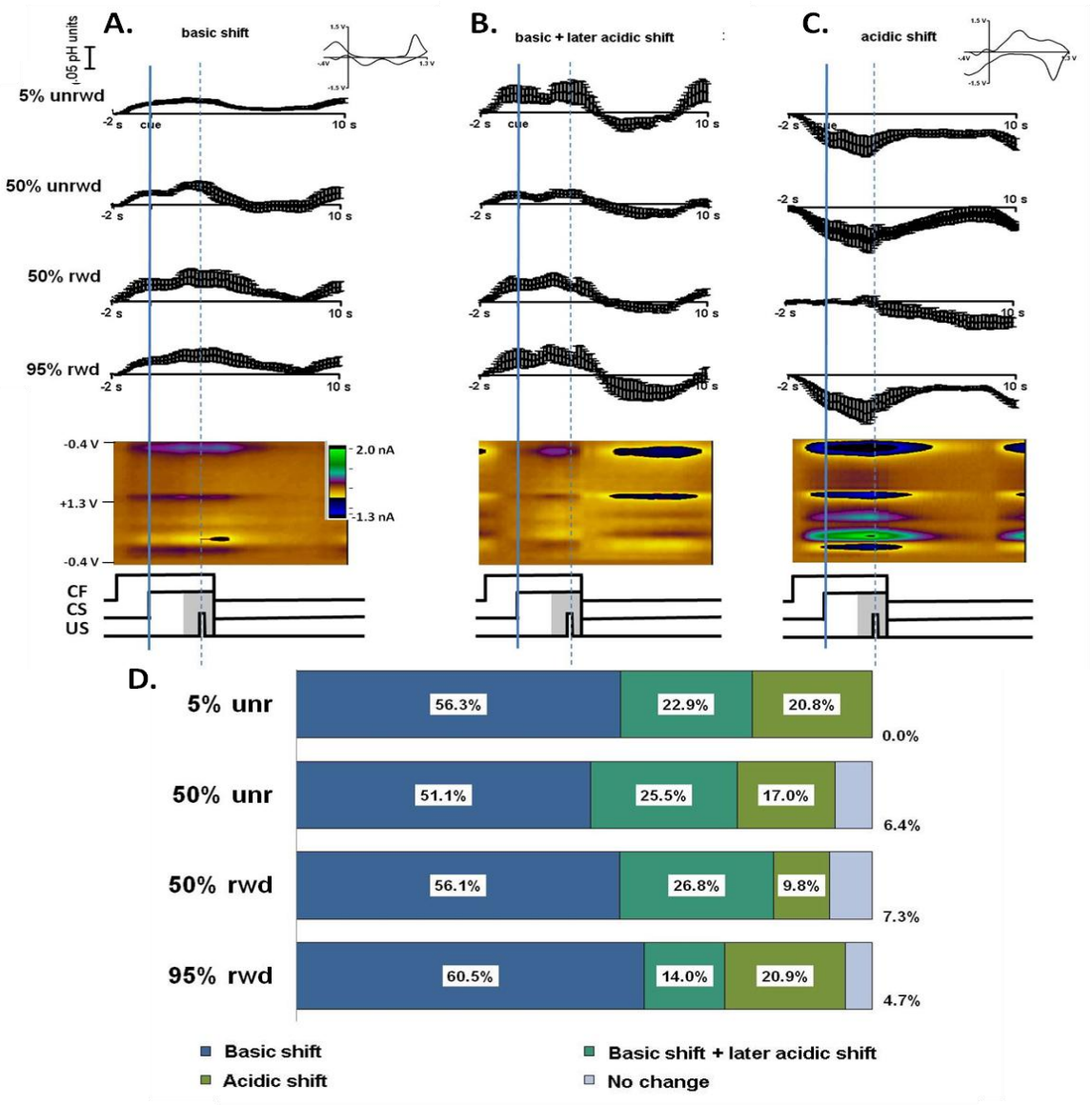

Figure 2.5. In vivo response to cues predicting different probabilities of reward. Average concentration v time traces for basic pH shift (A), basic followed by a later acidic pH shift (B), and an acidic shift type of response presented according to the cue predicting the probability of reward, 5% unrewarded trials, 50% unrewarded trials, 50% rewarded trials, and 95% rewarded trials. Below these traces is a representative color plot for each type of response above a simplified behavioral diagram. The cue was initiated at timestamp 0 s and the reward was delivered along dotted line (in rewarded trials). D. A summary of the percentage of responses by probability cue type. The largest number of responses were basic shifts pictured In blue and turquoise, followed by acidic shifts, either short term in green or long term in turquoise. A small percentage of responses showed no change (in purple).

uncertainty, where the 50% probability of reward cue predicts the highest uncertainty and the 5% and 95% predicts the lowest uncertainty for reward. There was not a significant difference in amplitude, 0.047 ± SEM for 50% probability trials and 0.078 ± SEM for 5 and 95% trials, but the data do suggest that there is a trend that a larger acidic pH shift is associated with lower uncertainty.

DISCUSSION

The aim of the present study was to assess the electrochemical changes that occur in primate striatum during reward-based behavioral paradigms. Fast-scan cyclic voltammetry offers the spatial and temporal resolution necessary to capture these electrochemical events *in vivo* in awake and behaving primates whereas conventional methods for measuring pH and catecholamine responses in the brain are not as rapid. Based on previous work conducted using electrophysiology and fMRI and in awake and freely moving rats, we hypothesized that there would be oxygen changes following the reward and that observing alkaline and acidic pH changes to the cue and reward *in vivo* would offer new information on the neurochemical changes that result because of neural activity. Secondary to that goal, we also hypothesized that there would be dopamine release to the cue and the reward as previously described by electrophysiology and electrochemistry (Schultz, 2002; Phillips et al., 2003; Cheer et al., 2006; Day et al., 2007; Roitman et al., 2008; Aragona et al., 2009; Owesson-White et al., 2009; Beyene et al., 2010; Jones et al., 2010; Wheeler et al., 2011). The major findings of this study are two-fold: acidic and alkaline pH shifts and oxygen changes were observed during cue and reward presentation and these responses overshadowed dopaminergic responses.

Extracellular oxygen concentrations in the brain are the balance between that consumed by ongoing respiration and that generated by increases in blood flow. In turn, oxygen and pH are coupled in the brain such that increases in oxygen as a result of

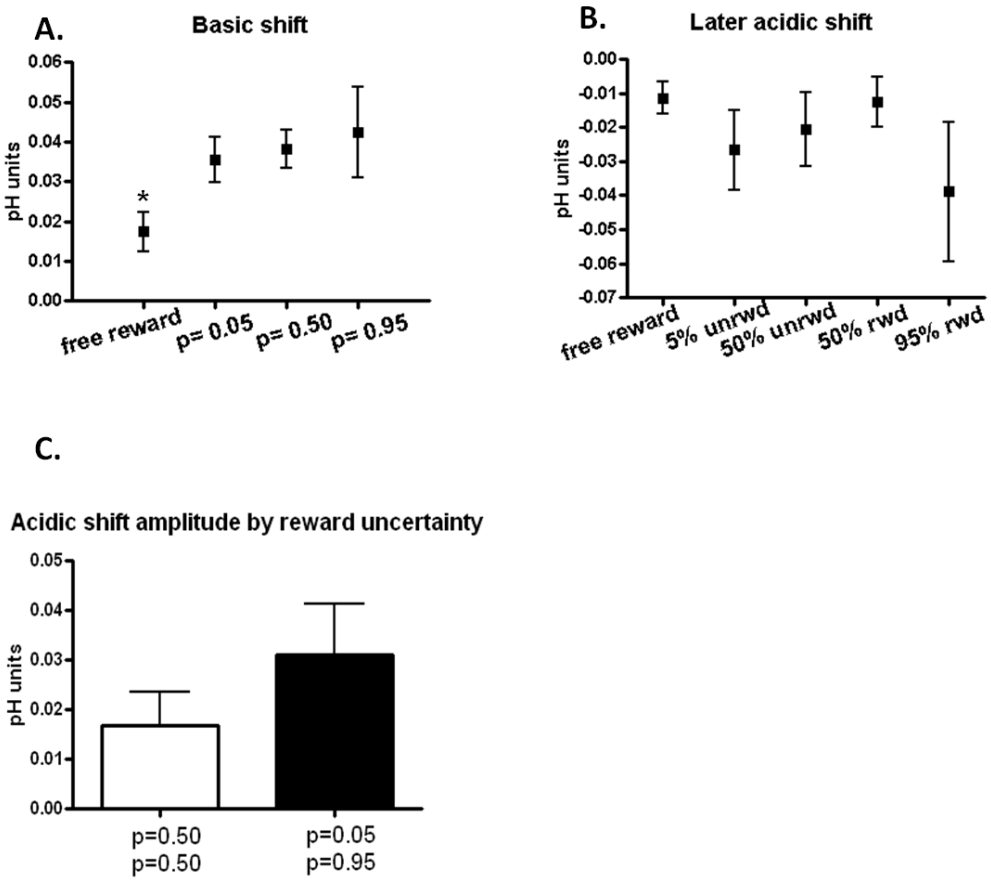

Figure 2.6. Basic and Acidic pH peak amplitude. A. Peak amplitudes for responses that showed a basic pH shift following the cue presentation. Peak amplitudes were taken at approximately 1.5 s after the cue presentation. B. Peak amplitudes for the later acidic pH shift following the basic pH shift. Peak amplitudes were taken between 6.0 and 7.0 s following the cue presentation. C. Peak amplitudes of acidic pH shift following the cue reported according to uncertainty. Rewarded and unrewarded trials following at cue that predicted 50% reward probability are grouped together as they have the same uncertainty value. Rewarded and unrewarded trials following the p=0.05 and p=0.95 are shown in black.

either enhanced blood flow or increased metabolism also increases pH. The pH of the extracellular fluid is governed by the buffering system of H_2CO_3/HCO_3^-. The concentration of H_2CO_3.is in equilibrium with the CO_2 concentration, a process that is controlled by carbonic anhydrase. Due to this equilibrium, acidic pH shifts are caused by an increase in the partial pressure of CO_2 arising from the oxidation of glucose either anaerobically, with the production of lactic acid and carbon dioxide, or aerobically with the production of carbon dioxide (Kaila, 1998; Chesler, 2003). The partial pressure of CO_2 is also dependent on cerebral blood flow that increases after neural activity. Increased blood flow clears CO_2 and delivers oxygen to the localized brain region causing an alkaline pH shift (Urbanics et al., 1978). Indeed, previous work using fast-scan cyclic voltammetry has coupled the complex balance of neural activity, CO_2 production and oxygen delivery, and pH shift. Venton and coworkers demonstrated that stimulation of dopaminergic neurons in the substantia nigra induce time-locked basic pH shifts and oxygen changes that were delayed approximately 2 seconds post-stimulation (Venton et al., 2003a).

Thus, the neural activity that accompanies reward-based activities should be accompanied by pH and O_2 concentration changes. Indeed, during unanticipated administration of a natural reward, alkaline shifts have been observed after dopamine release (Roitman et al., 2004). Thus, the short term alkaline shifts observed followed by a long term acidic shift in the striatum during free reward delivery (Figure 4) were anticipated. Previous work using ion selective electrodes reports long term acidic shifts preceded by short term basic shifts *in vivo* in the cerebellar cortex where neuronal circuits are well defined (Kraig et al., 1983; Somjen, 1984). In our work, the alkaline shift was significantly smaller than the amplitude of this shift during trials where a cue predicted with some probability, a juice reward, but there was no difference in the acidic pH response (Figure 6). This suggests that the increase in anaerobic glucose

consumption (metabolism), subsequent lactic acid increase, and overall, localized pH decrease coupled with the accompanying blood flow change did not differ significantly from the response seen in trials where a reward was delivered (or not) following a cue. The initial basic shift may rely largely on the cue that predicts the reward, varying linearly by probability, and that in the case where a reward is delivered without a deliberate cue (as the environment or timing of free reward block set of trials acts as an indirect cue in and of itself), the predominant response is an acidic shift to the reward delivery. In fact, because there is a time-locked response between oxygen change and pH in the extracellular fluid (increases in oxygen associated with increases in pH), our results correlate well with imaging techniques such as PET and fMRI (Raichle, 1998).

There are three predominant components to an fMRI signal: the initial dip, principal peak, and post-stimulus undershoot (Huettel SA, 2009). The physiological component of the principal peak is due to increases in cerebral blood flow which would cause a transient alkaline shift. Indeed, previous studies have shown neuronal activation in striatal neurons following unexpected (free) reward with electrophysiological measurements and human fMRI imaging (Berns et al., 2001). Time traces of neuronal activity in the caudate nucleus obtained with fMRI imaging during reward delivery show an increase in signal intensity at the beginning of a trial and at the presentation of a reward-predicting cue (Delgado et al., 2000; Zink et al., 2004). The increase in fMRI signal that correlates with the basic responses observed here lasts until between 1 and 3 seconds following the reward delivery. The fMRI signal returns to baseline after approximately 9 to 12 seconds along a similar time course reported in this study.

The most predominant response in the predicted reward trials was a short term basic shift (Figure 5). Additionally, the amplitude of this shift increased following the cue presentation and by probability of reward (Figure 6A). If the basic shift is an indicator of an increase in cerebral blood flow, then an increase or decrease in amplitude may serve

as an indirect measurement for neural activity and may correlate with the principal peak of fMRI studies. Additionally, previous evidence suggests that dopamine neurons encode errors in the prediction of reward (Fiorillo et al., 2003). Prediction error is the difference between the probability of reward delivery, represented by a distinct visual cue, and the actual outcome, rewarded or unrewarded trials. When the probability of reward is varied between 0 and 1, as in the case where cues represent probabilities of 5%, 50%, and 95%, uncertainty is introduced. Uncertainty is greatest during 50% probability trials and lowest (and equal) in 5% or 95% probability trials. Electrophysiological data suggests that dopaminergic responses to uncertainty are critical for decision making and that this neural activity increases to the cue according to increased probability of reward and decreases by probability time-locked to the reward event (in rewarded and unrewarded trials similarly) (Fiorillo et al., 2003).

The second most predominant response of the trials where a cue predicted the probability of a reward was an acidic shift following the basic shift (Figure 5). The physiological basis of this response is likely due to an increase in metabolism following neural activity. The time-course for this response aligns with the undershoot component of the fMRI signal (Frahm et al., 2008; Dechent et al., 2011). The peak amplitude of the pH shift in trials that showed this acidic shift was not different in rewarded and unrewarded trials, but did show a trend towards increasing with decreasing with uncertainty (Figure 6).

However, this evidence does not account for the approximately ~17% of responses that showed an *initial acidic* pH shift following the cue presentation. Direct measurements with oxygen sensors (Thompson et al., 2003) and BOLD fMRI (Kim et al., 2000) have shown that there is a fast increase in deoxyhemoglobin coinciding with neuronal activity followed by a delayed increase in oxygen levels. Though it is not always a measurable component of the fMRI signal, this initial dip is thought to be a

better direct indicator of neuronal activity than the principal peak which may work in corroboration with increases in cerebral blow flow (Ances, 2004; Buxton et al., 2004). Additionally, some studies connect the initial dip with the depletion of mitochondrial oxygen buffers caused by increased neuronal activity (Aubert and Costalat, 2002). The initial dip does not always proceed the peak in fMRI studies and could account for the for the small percentage of *initial* acidic responses observed here (Blanchard et al., 2011).

Dopamine-like signal during reward delivery

In the 50 % reward probability in animal 3 and in 14 % of the free reward studies in animals 2 and 3, dopamine-like signals were obtained. Validation of an *in vivo* signal requires that five criteria be met. These include cyclic voltammograms that match ones for authentic cyclic voltammograms of the species detected, anatomical and physiological verification, pharmacological characterization of the signal, and an independent chemical analysis (Phillips and Wightman, 2003). In the monkey model, according to animal use policies, we were not able to verify the dopamine-like signal with pharmacological characterization or via electrical stimulation as in previous studies in rodents (Cahill et al., 1996; Phillips and Wightman, 2003; Robinson and Wightman, 2007) . The inability to electrically stimulate primate dopamine cell bodies *in vivo* prevents the use of principal component regression analysis of the dopamine-like analyte or the reduction of oxygen at our electrode. Dopamine release at terminal sites has been well characterized in the putamen (Cragg et al., 2002), and oxygen increases following stimulation have been studied as well (Zimmerman et al., 1992; Venton et al., 2003a; Cheer et al., 2006). The oxidation and reduction peaks of this signal (Figures 3 and 4) match closely with the *in vitro* quantification of dopamine when the characteristics with the different waveforms are considered (Figure 2) (r^2=0.84). Similarly, the *in vivo* O_2 signal (Figure 3) shows close agreement with that obtained *in vitro*. The cyclic voltammograms attributed to pH changes (Figure 4) also showed close correlation with

those recorded under known conditions. Finally, the electrode locations in the putamen were verified with post-mortem histological reconstructions (Paxinos, 2000). Therefore, several of the criteria for identifying these species have been met.

In animal 3, with the cue predicting a 0.5 reward probability there was a significant increase after the reward at the dopamine potential for rewarded trials that was similar in time scale to previously reported for natural rewards (Roitman et al., 2004) ($p<0.001$, Student's t-test) (Figure 3A). We observed a slight increase in the cue-induced dopamine though it did not exceed the baseline for noise in rewarded and unrewarded trials. Interestingly, there was an oxygen increase following the reward (or not in unrewarded trials), but there was not a significant difference between the two signals. Oxygen increases have been reported in rodent models following stimulation, but have not been reported in primates during natural reward (Venton et al., 2003a). Previous work suggests that a signal attributable to dopamine increases to unexpected rewards but we did not see this in this animal.

It was possible to measure dopamine-like changes in a small number of locations during free reward delivery with this waveform in animals 2 and 3. Electrophysiology data shows that dopamine neurons burst fire during reward delivery (Schultz, 2002; Robinson et al., 2008). The burst firing of dopamine neurons is expected to cause phasic concentrations in the terminal regions (Runnels et al., 1999; Sombers et al., 2009). A recent study shows that selectively activating ventral tegmental area neurons that terminate in the striatum is enough to mediate behavioral conditioning in rats (Tsai et al., 2009). Here, the dopamine release during free reward was elevated for about one second, which is on the time scale previously reported for naturally occurring transient dopamine release (Wightman and Robinson, 2002; Robinson et al., 2003; Wightman et al., 2007), but are faster than previous reports of dopamine release during natural reward delivery (Roitman et al., 2004). This might be due to the potential overlap of

signaling between the pH and dopamine components over time. Mostly likely, it is due to the differences in dopamine uptake rate in rats compared to primates. The dopamine uptake rates measured in the striatum of primate brain slices report a V_{max} double compared to the V_{max} in rodents (Cragg et al., 2000, 2002). A higher uptake rate explains the shorter time course measured during free reward delivery and demonstrates the difficultly for measuring dopamine release in primates compared to rodents, as clearance of dopamine from the extracellular space is faster.

Another difference between rodent and primate brains that may account for the heterogeneity of responses has to do with the distribution of blood vessels throughout the primate brain. The intercapillary distance in primate cortex is 60 µm and 100 µm in the grey matter (Levin et al., 1976). The maximum diameter of our electrodes was 33 µm and as such, could be placed closer or further way from a site of neural activity or a blood vessel during any given recording. According to the model, an electrode placed closer to a site of neural activity would record acidic pH changes and an electrode placed closer to a blood vessel would likely measure alkaline pH changes more readily. Furthermore, previous reports on pH have been performed in the rodent in which the intercapillary distance is ~50 µm (LaManna et al., 2004). The increased diffusion distance to the electrode in the primate brain and the relative location of the electrode to capillaries or activation sites could account for the larger acidic and alkaline shifts compared to rodent studies However, cortical respiration rates in primates is lower than in rodents (Attwell and Laughlin, 2001).

Summary

We have demonstrated that fast-scan cyclic voltammetry with the carbon-fiber microelectrode is a useful tool for measuring catecholamine, pH, and oxygen signals in the primate striatum. At some locations a dopamine-like signal was measured to the cue

and to the reward during p=0.50 reward trials and in free reward trials directly following the reward. Additionally, we have shown two correlates for differential pH changes in the brain, as an indicator for oxygen delivery and neural activity in the case of basic pH changes and in the case of acidic pH changes we assume an increase in glucose consumption and CO_2. Further studies with a blood flow sensor are necessary to further elucidate the link between neural activity, metabolism and blood flow, pH, and fMRI studies.

REFERENCES

Aguirre GK, Zarahn E, D'Esposito M (1998) The variability of human, BOLD hemodynamic responses. Neuroimage 8:360-369.

Ances BM (2004) Coupling of changes in cerebral blood flow with neural activity: what must initially dip must come back up. J Cereb Blood Flow Metab 24:1-6.

Aragona BJ, Day JJ, Roitman MF, Cleaveland NA, Wightman RM, Carelli RM (2009) Regional specificity in the real-time development of phasic dopamine transmission patterns during acquisition of a cue-cocaine association in rats. Eur J Neurosci 30:1889-1899.

Attwell D, Laughlin SB (2001) An energy budget for signaling in the grey matter of the brain. J Cereb Blood Flow Metab 21:1133-1145.

Aubert A, Costalat R (2002) A model of the coupling between brain electrical activity, metabolism, and hemodynamics: application to the interpretation of functional neuroimaging. Neuroimage 17:1162-1181.

Bandettini PA, Jesmanowicz A, Wong EC, Hyde JS (1993) Processing strategies for time-course data sets in functional MRI of the human brain. Magn Reson Med 30:161-173.

Bermudez MA, Schultz W (2010) Reward magnitude coding in primate amygdala neurons. J Neurophysiol 104:3424-3432.

Berns GS, McClure SM, Pagnoni G, Montague PR (2001) Predictability modulates human brain response to reward. J Neurosci 21:2793-2798.

Beyene M, Carelli RM, Wightman RM (2010) Cue-evoked dopamine release in the nucleus accumbens shell tracks reinforcer magnitude during intracranial self-stimulation. Neuroscience 169:1682-1688.

Blanchard S, Papadopoulo T, Benar CG, Voges N, Clerc M, Benali H, Warnking J, David O, Wendling F (2011) Relationship between flow and metabolism in BOLD signals: insights from biophysical models. Brain Topogr 24:40-53.

Brown JH, Makman MH (1972) Stimulation by dopamine of adenylate cyclase in retinal homogenates and of adenosine-3':5'-cyclic monophosphate formation in intact retina. Proc Natl Acad Sci U S A 69:539-543.

Buxton RB, Uludag K, Dubowitz DJ, Liu TT (2004) Modeling the hemodynamic response to brain activation. Neuroimage 23 Suppl 1:S220-233.

Caesar K, Hashemi P, Douhou A, Bonvento G, Boutelle MG, Walls AB, Lauritzen M (2008) Glutamate receptor-dependent increments in lactate, glucose and oxygen metabolism evoked in rat cerebellum in vivo. J Physiol 586:1337-1349.

Cahill PS, Walker QD, Finnegan JM, Mickelson GE, Travis ER, Wightman RM (1996) Microelectrodes for the measurement of catecholamines in biological systems. Anal Chem 68:3180-3186.

Cheer JF, Wassum KM, Wightman RM (2006) Cannabinoid modulation of electrically evoked pH and oxygen transients in the nucleus accumbens of awake rats. J Neurochem 97:1145-1154.

Chen JC, Chesler M (1992a) pH transients evoked by excitatory synaptic transmission are increased by inhibition of extracellular carbonic anhydrase. Proc Natl Acad Sci U S A 89:7786-7790.

Chen JC, Chesler M (1992b) Extracellular alkaline shifts in rat hippocampal slice are mediated by NMDA and non-NMDA receptors. J Neurophysiol 68:342-344.

Chesler M (2003) Regulation and modulation of pH in the brain. Physiol Rev 83:1183-1221.

Clark LC, Jr., Wolf R, Granger D, Taylor Z (1953) Continuous recording of blood oxygen tensions by polarography. J Appl Physiol 6:189-193.

Cragg SJ, Rice ME (2004) DAncing past the DAT at a DA synapse. Trends Neurosci 27:270-277.

Cragg SJ, Hille CJ, Greenfield SA (2000) Dopamine release and uptake dynamics within nonhuman primate striatum in vitro. J Neurosci 20:8209-8217.

Cragg SJ, Hille CJ, Greenfield SA (2002) Functional domains in dorsal striatum of the nonhuman primate are defined by the dynamic behavior of dopamine. J Neurosci 22:5705-5712.

Day JJ, Roitman MF, Wightman RM, Carelli RM (2007) Associative learning mediates dynamic shifts in dopamine signaling in the nucleus accumbens. Nat Neurosci 10:1020-1028.

De Camilli P, Macconi D, Spada A (1979) Dopamine inhibits adenylate cyclase in human prolactin-secreting pituitary adenomas. Nature 278:252-254.

Dechent P, Schutze G, Helms G, Merboldt KD, Frahm J (2011) Basal cerebral blood volume during the poststimulation undershoot in BOLD MRI of the human brain. J Cereb Blood Flow Metab 31:82-89.

Delgado MR, Nystrom LE, Fissell C, Noll DC, Fiez JA (2000) Tracking the hemodynamic responses to reward and punishment in the striatum. J Neurophysiol 84:3072-3077.

Di Chiara G, Imperato A (1988) Drugs abused by humans preferentially increase synaptic dopamine concentrations in the mesolimbic system of freely moving rats. Proc Natl Acad Sci U S A 85:5274-5278.

Fields HL, Hjelmstad GO, Margolis EB, Nicola SM (2007) Ventral tegmental area neurons in learned appetitive behavior and positive reinforcement. Annu Rev Neurosci 30:289-316.

Fiorillo CD, Tobler PN, Schultz W (2003) Discrete coding of reward probability and uncertainty by dopamine neurons. Science 299:1898-1902.

Forry SP, Murray JR, Heien ML, Locascio LE, Wightman RM (2004) Probing electric fields inside microfluidic channels during electroosmotic flow with fast-scan cyclic voltammetry. Anal Chem 76:4945-4950.

Fox PT, Mintun MA, Raichle ME, Miezin FM, Allman JM, Van Essen DC (1986) Mapping human visual cortex with positron emission tomography. Nature 323:806-809.

Frahm J, Baudewig J, Kallenberg K, Kastrup A, Merboldt KD, Dechent P (2008) The post-stimulation undershoot in BOLD fMRI of human brain is not caused by elevated cerebral blood volume. Neuroimage 40:473-481.

Garris PA, Christensen JR, Rebec GV, Wightman RM (1997) Real-time measurement of electrically evoked extracellular dopamine in the striatum of freely moving rats. J Neurochem 68:152-161.

Garris PA, Budygin EA, Phillips PE, Venton BJ, Robinson DL, Bergstrom BP, Rebec GV, Wightman RM (2003) A role for presynaptic mechanisms in the actions of nomifensine and haloperidol. Neuroscience 118:819-829.

Grace AA, Onn SP (1989) Morphology and electrophysiological properties of immunocytochemically identified rat dopamine neurons recorded in vitro. J Neurosci 9:3463-3481.

Haber SN, Fudge JL (1997) The primate substantia nigra and VTA: integrative circuitry and function. Crit Rev Neurobiol 11:323-342.

Hashemi P, Dankoski EC, Petrovic J, Keithley RB, Wightman RM (2009) Voltammetric detection of 5-hydroxytryptamine release in the rat brain. Anal Chem 81:9462-9471.

Heien ML, Johnson MA, Wightman RM (2004) Resolving neurotransmitters detected by fast-scan cyclic voltammetry. Anal Chem 76:5697-5704.

Heien ML, Phillips PE, Stuber GD, Seipel AT, Wightman RM (2003a) Overoxidation of carbon-fiber microelectrodes enhances dopamine adsorption and increases sensitivity. Analyst 128:1413-1419.

Heien ML, Khan AS, Ariansen JL, Cheer JF, Phillips PE, Wassum KM, Wightman RM (2005) Real-time measurement of dopamine fluctuations after cocaine in the brain of behaving rats. Proc Natl Acad Sci U S A 102:10023-10028.

Heien MLAV (2005) Probing dopamine release and function with carbon-fiber microelectrodes. In. Chapel Hill: The University of North Carolina at Chapel Hill.

Heien MLAV, Phillips PEM, Stuber GD, Seipel AT, Wightman RM (2003b) Overoxidation of carbon-fiber microelectrodes enhances dopamine adsorption and increases sensitivity. Analyst 128:1413-1419.

Herculano-Houzel S (2009) The human brain in numbers: a linearly scaled-up primate brain. Front Hum Neurosci 3:31.

Hermans A (2007) Fabrication and applications of dopamine-sensitive electrodes. In. Chapel Hill: The University of North Carolinat at Chapel Hlll.

Hermans A, Wightman RM (2006) Conical tungsten tips as substrates for the preparation of ultramicroelectrodes. Langmuir 22:10348-10353.

Hermans A, Seipel AT, Miller CE, Wightman RM (2006) Carbon-fiber microelectrodes modified with 4-sulfobenzene have increased sensitivity and selectivity for catecholamines. Langmuir 22:1964-1969.

Huettel SA SA, and Gregory McCarthy (2009) Functional Magnetic Resonance Imaging, 2nd Edition. Sunderland, MA: Sinauer Associates, Inc.

Hyland BI, Reynolds JN, Hay J, Perk CG, Miller R (2002) Firing modes of midbrain dopamine cells in the freely moving rat. Neuroscience 114:475-492.

Ikemoto S (2007) Dopamine reward circuitry: two projection systems from the ventral midbrain to the nucleus accumbens-olfactory tubercle complex. Brain Res Rev 56:27-78.

Ikemoto S, Glazier BS, Murphy JM, McBride WJ (1997) Role of dopamine D1 and D2 receptors in the nucleus accumbens in mediating reward. J Neurosci 17:8580-8587.

Jaquins-Gerstl A, Michael AC (2009) Comparison of the brain penetration injury associated with microdialysis and voltammetry. J Neurosci Methods 183:127-135.

Jones JL, Day JJ, Aragona BJ, Wheeler RA, Wightman RM, Carelli RM (2010) Basolateral amygdala modulates terminal dopamine release in the nucleus accumbens and conditioned responding. Biol Psychiatry 67:737-744.

Jones SR, Joseph JD, Barak LS, Caron MG, Wightman RM (1999) Dopamine neuronal transport kinetics and effects of amphetamine. J Neurochem 73:2406-2414.

Kaila K, Ransom, B. R. (1998) pH and Brain Function. New York: Wiley-Liss.

Kauer JA, Malenka RC (2007) Synaptic plasticity and addiction. Nat Rev Neurosci 8:844-858.

Kawagoe KT, Zimmerman JB, Wightman RM (1993) Principles of voltammetry and microelectrode surface states. J Neurosci Meth 48:225-240.

Kebabian JW, Calne DB (1979) Multiple receptors for dopamine. Nature 277:93-96.

Keithley RB, Heien ML, Wightman RM (2009) Multivariate concentration determination using principal component regression with residual analysis. Trends Analyt Chem 28:1127-1136.

Keithley RB, Takmakov P, Bucher ES, Belle AM, Owesson-White CA, Park J, Wightman RM (2011) Higher sensitivity dopamine measurements with faster-scan cyclic voltammetry. Anal Chem 83:3563-3571.

Kim DS, Duong TQ, Kim SG (2000) High-resolution mapping of iso-orientation columns by fMRI. Nat Neurosci 3:164-169.

Kraig RP, Ferreira-Filho CR, Nicholson C (1983) Alkaline and acid transients in cerebellar microenvironment. J Neurophysiol 49:831-850.

LaManna JC, Chavez JC, Pichiule P (2004) Structural and functional adaptation to hypoxia in the rat brain. J Exp Biol 207:3163-3169.

Levin VA, Landahl HD, Freeman-Dove MA (1976) The application of brain capillary permeability coefficient measurements to pathological conditions and the selection of agents which cross the blood-brain barrier. J Pharmacokinet Biopharm 4:499-519.

Lu Y, Peters JL, Michael AC (1998) Direct comparison of the response of voltammetry and microdialysis to electrically evoked release of striatal dopamine. J Neurochem 70:584-593.

Margolis EB, Lock H, Hjelmstad GO, Fields HL (2006) The ventral tegmental area revisited: is there an electrophysiological marker for dopaminergic neurons? J Physiol 577:907-924.

Michael D, Travis ER, Wightman RM (1998) Color images for fast-scan CV. Analytical Chemistry 70:586a-592a.

Michael DJ, Joseph JD, Kilpatrick MR, Travis ER, Wightman RM (1999) Improving data acquisition for fast scan cyclic voltammetry. Analytical Chemistry 71:3941-3947.

Nowak LG, Bullier J (1998) Axons, but not cell bodies, are activated by electrical stimulation in cortical gray matter. II. Evidence from selective inactivation of cell bodies and axon initial segments. Exp Brain Res 118:489-500.

O'Doherty JP (2004) Reward representations and reward-related learning in the human brain: insights from neuroimaging. Curr Opin Neurobiol 14:769-776.

Ogawa S, Lee TM, Kay AR, Tank DW (1990) Brain magnetic resonance imaging with contrast dependent on blood oxygenation. Proc Natl Acad Sci U S A 87:9868-9872.

Onn SP, West AR, Grace AA (2000) Dopamine-mediated regulation of striatal neuronal and network interactions. Trends Neurosci 23:S48-56.

Overton PG, Clark D (1997) Burst firing in midbrain dopaminergic neurons. Brain Res Brain Res Rev 25:312-334.

Owesson-White CA, Cheer JF, Beyene M, Carelli RM, Wightman RM (2008) Dynamic changes in accumbens dopamine correlate with learning during intracranial self-stimulation. Proc Natl Acad Sci U S A 105:11957-11962.

Owesson-White CA, Ariansen J, Stuber GD, Cleaveland NA, Cheer JF, Wightman RM, Carelli RM (2009) Neural encoding of cocaine-seeking behavior is coincident with phasic dopamine release in the accumbens core and shell. Eur J Neurosci 30:1117-1127.

Park J, Kile BM, Wightman RM (2009) In vivo voltammetric monitoring of norepinephrine release in the rat ventral bed nucleus of the stria terminalis and anteroventral thalamic nucleus. Eur J Neurosci 30:2121-2133.

Parsons LH, Justice JB, Jr. (1992) Extracellular concentration and in vivo recovery of dopamine in the nucleus accumbens using microdialysis. J Neurochem 58:212-218.

Paxinos G, Huang, X, and Toga, AW (2000) The Rhesus Monkey Brain in Stereotaxic Coordinates. New York: Academic

Phillips PE, Stuber GD, Heien ML, Wightman RM, Carelli RM (2003) Subsecond dopamine release promotes cocaine seeking. Nature 422:614-618.

Phillips PEM, Wightman RM (2003) Critical guidelines for validation of the selectivity of in-vivo chemical microsensors. TrAC Trends in Analytical Chemistry 22:509-514.

Raichle ME (1998) Behind the scenes of functional brain imaging: a historical and physiological perspective. Proc Natl Acad Sci U S A 95:765-772.

Richfield EK, Penney JB, Young AB (1989) Anatomical and affinity state comparisons between dopamine D1 and D2 receptors in the rat central nervous system. Neuroscience 30:767-777.

Robinson DL, Wightman RM (2007) Rapid Dopamine Release in Freely Moving Rats.

Robinson DL, Venton BJ, Heien ML, Wightman RM (2003) Detecting subsecond dopamine release with fast-scan cyclic voltammetry in vivo. Clin Chem 49:1763-1773.

Robinson DL, Hermans A, Seipel AT, Wightman RM (2008) Monitoring rapid chemical communication in the brain. Chem Rev 108:2554-2584.

Robinson DL, Phillips PE, Budygin EA, Trafton BJ, Garris PA, Wightman RM (2001) Sub-second changes in accumbal dopamine during sexual behavior in male rats. Neuroreport 12:2549-2552.

Roitman MF, Wheeler RA, Wightman RM, Carelli RM (2008) Real-time chemical responses in the nucleus accumbens differentiate rewarding and aversive stimuli. Nat Neurosci 11:1376-1377.

Roitman MF, Stuber GD, Phillips PE, Wightman RM, Carelli RM (2004) Dopamine operates as a subsecond modulator of food seeking. J Neurosci 24:1265-1271.

Runnels PL, Joseph JD, Logman MJ, Wightman RM (1999) Effect of pH and surface functionalities on the cyclic voltammetric responses of carbon-fiber microelectrodes. Anal Chem 71:2782-2789.

Schmitz Y, Lee CJ, Schmauss C, Gonon F, Sulzer D (2001) Amphetamine distorts stimulation-dependent dopamine overflow: effects on D2 autoreceptors, transporters, and synaptic vesicle stores. J Neurosci 21:5916-5924.

Schultz W (2002) Getting formal with dopamine and reward. Neuron 36:241-263.

Schultz W, Dayan P, Montague PR (1997) A neural substrate of prediction and reward. Science 275:1593-1599.

Shepard PD, Bunney BS (1988) Effects of apamin on the discharge properties of putative dopamine-containing neurons in vitro. Brain Res 463:380-384.

Sombers LA, Beyene M, Carelli RM, Wightman RM (2009) Synaptic overflow of dopamine in the nucleus accumbens arises from neuronal activity in the ventral tegmental area. J Neurosci 29:1735-1742.

Somjen GG (1984) Acidification of interstitial fluid in hippocampal formation caused by seizures and by spreading depression. Brain Res 311:186-188.

Stamford JA, Kruk ZL, Millar J, Wightman RM (1984) Striatal dopamine uptake in the rat: in vivo analysis by fast cyclic voltammetry. Neurosci Lett 51:133-138.

Stuber GD, Roitman MF, Phillips PE, Carelli RM, Wightman RM (2005) Rapid dopamine signaling in the nucleus accumbens during contingent and noncontingent cocaine administration. Neuropsychopharmacology 30:853-863.

Takmakov P, Zachek MK, Keithley RB, Bucher ES, McCarty GS, Wightman RM (2010) Characterization of local pH changes in brain using fast-scan cyclic voltammetry with carbon microelectrodes. Anal Chem 82:9892-9900.

Thompson JK, Peterson MR, Freeman RD (2003) Single-neuron activity and tissue oxygenation in the cerebral cortex. Science 299:1070-1072.

Tobler PN, Dickinson A, Schultz W (2003) Coding of predicted reward omission by dopamine neurons in a conditioned inhibition paradigm. J Neurosci 23:10402-10410.

Tobler PN, Fiorillo CD, Schultz W (2005) Adaptive coding of reward value by dopamine neurons. Science 307:1642-1645.

Tobler PN, O'Doherty JP, Dolan RJ, Schultz W (2007) Reward value coding distinct from risk attitude-related uncertainty coding in human reward systems. J Neurophysiol 97:1621-1632.

Tobler PN, Christopoulos GI, O'Doherty JP, Dolan RJ, Schultz W (2009) Risk-dependent reward value signal in human prefrontal cortex. Proc Natl Acad Sci U S A 106:7185-7190.

Tsai HC, Zhang F, Adamantidis A, Stuber GD, Bonci A, de Lecea L, Deisseroth K (2009) Phasic firing in dopaminergic neurons is sufficient for behavioral conditioning. Science 324:1080-1084.

Urbanics R, Leniger-Follert E, Lubbers DW (1978) Time course of changes of extracellular H+ and K+ activities during and after direct electrical stimulation of the brain cortex. Pflugers Arch 378:47-53.

Venton BJ, Michael DJ, Wightman RM (2003a) Correlation of local changes in extracellular oxygen and pH that accompany dopaminergic terminal activity in the rat caudate-putamen. J Neurochem 84:373-381.

Venton BJ, Zhang H, Garris PA, Phillips PE, Sulzer D, Wightman RM (2003b) Real-time decoding of dopamine concentration changes in the caudate-putamen during tonic and phasic firing. J Neurochem 87:1284-1295.

Verhagen JV, Gabbott PL, Rolls ET (2003) A simple method for reconditioning epoxy-coated microelectrodes for extracellular single neuron recording. J Neurosci Meth 123:215-217.

Westerink BH (1995) Brain microdialysis and its application for the study of animal behaviour. Behav Brain Res 70:103-124.

Wheeler RA, Aragona BJ, Fuhrmann KA, Jones JL, Day JJ, Cacciapaglia F, Wightman RM, Carelli RM (2011) Cocaine cues drive opposing context-dependent shifts in reward processing and emotional state. Biol Psychiatry 69:1067-1074.

Wightman RM, Robinson DL (2002) Transient changes in mesolimbic dopamine and their association with 'reward'. J Neurochem 82:721-735.

Wightman RM, May LJ, Michael AC (1988) Detection of dopamine dynamics in the brain. Anal Chem 60:769A-779A.

Wightman RM, Heien ML, Wassum KM, Sombers LA, Aragona BJ, Khan AS, Ariansen JL, Cheer JF, Phillips PE, Carelli RM (2007) Dopamine release is heterogeneous within microenvironments of the rat nucleus accumbens. Eur J Neurosci 26:2046-2054.

Wise RA (2004) Dopamine, learning and motivation. Nat Rev Neurosci 5:483-494.

Wu Q, Reith ME, Walker QD, Kuhn CM, Carroll FI, Garris PA (2002) Concurrent autoreceptor-mediated control of dopamine release and uptake during neurotransmission: an in vivo voltammetric study. J Neurosci 22:6272-6281.

Yoshimi K, Naya Y, Mitani N, Kato T, Inoue M, Natori S, Takahashi T, Weitemier A, Nishikawa N, McHugh T, Einaga Y, Kitazawa S (2011) Phasic reward responses in the monkey striatum as detected by voltammetry with diamond microelectrodes. Neurosci Res.

Zimmerman JB, Kennedy RT, Wightman RM (1992) Evoked neuronal activity accompanied by transmitter release increases oxygen concentration in rat striatum in vivo but not in vitro. J Cereb Blood Flow Metab 12:629-637.

Zink CF, Pagnoni G, Martin-Skurski ME, Chappelow JC, Berns GS (2004) Human striatal responses to monetary reward depend on saliency. Neuron 42:509-517.